

Plasma acceleration by the interaction of parallel propagating Alfvén waves

F. MOTTEZ †

Laboratoire Univers et Théories (LUTH), Observatoire de Paris; CNRS UMR8102, Université Paris Diderot; 5 Place Jules Janssen, 92190 Meudon, France

(Received 9 October 2018)

It is shown that two circularly polarised Alfvén waves that propagate along the ambient magnetic field in an uniform plasma trigger non oscillating electromagnetic field components when they cross each other. The non-oscillating field components can accelerate ions and electrons with great efficiency. This work is based on particle-in-cell (PIC) numerical simulations and on analytical non-linear computations. The analytical computations are done for two counter-propagating monochromatic waves. The simulations are done with monochromatic waves and with wave packets. The simulations show parallel electromagnetic fields consistent with the theory, and they show that the particle acceleration result in plasma cavities and, if the waves amplitudes are high enough, in ion beams. These acceleration processes could be relevant in space plasmas. For instance, they could be at work in the auroral zone and in the radiation belts of the Earth magnetosphere. In particular, they may explain the origin of the deep plasma cavities observed in the Earth auroral zone.

1. Introduction

We investigate plasma acceleration based on the non-linear interaction of counter-propagating MHD waves. A first analysis was presented in Mottez (2012*a*). The present paper is devoted to a more thorough analysis of this process, that is now called Acceleration by Parallel Alfvén Waves Interactions (APAWI).

Most of the known Alfvénic acceleration mechanisms involve short perpendicular scales (Knudsen 2001; Mottez 2012*b*). For instance $k_{\perp}c/\omega_{pe} \sim 1$ (Goertz 1984; Thompson & Lysak 1996; Lysak & Song 2003*b*) or $k_{\perp}\rho_i \sim 1$ (Hasegawa & Mima 1978) where ρ_i is the ion Larmor radius and k_{\perp} is the wavelength in the direction orthogonal to the ambient magnetic field. At odds with all these processes, APAWI involves waves in parallel propagation to the magnetic field ($k_{\perp} = 0$). Because the magnetic field direction is a privileged direction of propagation of Alfvén waves, APAWI is potentially relevant in space plasma physics. The first paper was developed in connexion with acceleration in the Earth auroral zone. But it could be at work in any place where trapped or reflected Alfvén waves counter-propagate; for instance in the Earth radiation belts, or in closed magnetic loops in the solar corona.

The investigation of APAWI in (Mottez 2012*a*) was initially based on numerical simulations and completed with theoretical computations. In (Mottez 2012*a*), the numerical simulations put in evidence the settlement of non oscillatory parallel electric field (if the waves polarisation are appropriate), its bilinear dependence on the waves amplitudes, and the creation of plasma cavities. This last property was interpreted as a proxy of plasma

† Email address for correspondence: fabrice.mottez@obspm.fr

acceleration. A theoretical computation of the electric field parallel to \vec{B}_0 confirmed the existence of the non oscillatory component seen in the numerical simulations.

Both the numerical and the theoretical aspects of the problem are re-analysed here. The following points are studied more thoroughly.

A series of simulations has been conducted to complement those presented in Mottez (2012a). The simulations in the previous paper were conducted with a PIC code that computes electron guiding centre and full ion dynamics (Mottez *et al.* 1998). Did this code contain approximations that could have biased the physics? In order to answer that question, the simulations presented in the present paper are done with another PIC code where the electron full dynamics is taken into account. This code also allows simulations with lower ambient magnetic fields. The simulation are run over longer durations. All these differences are used to test the robustness of the acceleration mechanism presented in (Mottez 2012a).

The theory developed in (Mottez 2012a) showed the same wave interaction terms as in the simulations; but it showed also a few supplementary terms that did not appear in the simulations. These terms were proportional to the square of the amplitude of a *single* wave. Therefore, they were not associated with wave-wave interaction. We called them self-wave coupling terms and the drawback that they represented was not resolved in (Mottez 2012a). In section 3 and appendix A, we derive again the computation of the electric field along \vec{B}_0 developed in (Mottez 2012a), with the addition of the constraint associated with the Maxwell-Faraday law. It then appears that the self-wave-coupling terms disappear, and we obtain exactly what is seen in the numerical simulations.

Because of this reconsideration of the theoretical work, the reader can use the present paper as the fundamental paper describing the principle of APAWI. All the valid theory developed up to now is here. The former paper (Mottez 2012a) can be considered as a seminal paper. It is still interesting because of the parametric study conducted with numerical simulations (it is not repeated here) that allows for both qualitative and quantitative tests of the theory.

It might seem impossible that an electric field that is locally perpendicular to the magnetic field \vec{B} can accelerate particles in its average direction \vec{B}_0 . Nevertheless, acceleration occurs. The ability of APAWI to accelerate electrons and ions is demonstrated with simple analytical calculations in section 4.

A series of signatures that could help to characterise APAWI in observational data is presented in section 5.

In section 6, a few examples of published observations where APAWI might be relevant are discussed.

The main conclusions of our study as well as a short discussion relative to other theories involving parallel Alfvén waves interaction are presented in the last section.

2. Numerical method and simulation parameters

The physical variables are reduced to dimensionless variables. Time and frequencies are normalized by the electron plasma frequency ω_{p0} that correspond to a reference background electron density n_0 . Velocities are normalized to the speed of light c , and the magnetic field is given in terms of the dimensionless electron gyrofrequency ω_{ce}/ω_{p0} . The mass unit is the electron mass m_e . Therefore, the units (starting from the Maxwell Eq. in the MKSA system) are c/ω_{p0} for distances, ω_{p0}/c for wave vectors, e for charges, en_0 for the charge density, $c\omega_{ce}/\omega_{p0}$ for the electric field. In the following parts of this paper, numerical values and figures are expressed in this system of units.

For the understanding of APAWI, it is necessary to use simultaneously two systems of

coordinates. The coordinates system (X, Y, Z) is associated with the orthonormal basis $(\vec{e}_X, \vec{e}_Y, \vec{e}_Z)$ where \vec{e}_X is parallel to \vec{B}_0 . The unit vectors \vec{e}_Y, \vec{e}_Z are set arbitrarily, as long as they contribute with \vec{e}_X to form an orthonormal basis. In the approximation of a uniform magnetic field \vec{B}_0 applied in the computation, this coordinate system is time invariant and uniform. We can attach a local frame of reference to the local magnetic field $\vec{B}(X, t)$. The \vec{e}_x axis of this local frame of reference of coordinates (x, y, z) is parallel to the local magnetic field. For convenience, the basis $(\vec{e}_x, \vec{e}_y, \vec{e}_z)$ can be defined as the result of the rotation R_Z of axis \vec{e}_z and angle θ_Y of the set $(\vec{e}_X, \vec{e}_Y, \vec{e}_Z)$, followed by a rotation R_{Y1} of axis $e_{Y1} = R_Z(\vec{e}_y)$ and angle $-\theta_Z$.

This paper is based on a series of numerical simulations, whose naming convention is AWC (for Alfvén wave crossing) followed by a number, or a number and a letter. These simulation share most of their characteristics with AWC009, that is therefore used as a reference simulation.

In AWC009, two wave packets propagate in a uniform plasma. There are 1638400 particles of each species in the simulation; it corresponds to 100 particles per cell. There are 65536 time steps, defined by $\Delta t = 0.1$, corresponding to a time lapse $t_{max} = 6553.6$. The size of the whole simulation domain is $4096\Delta x \times 4\Delta y$, where $\Delta x = \Delta y = 0.10$ is the size of the grid cells. The electron thermal velocity is $v_{te} = 0.1$; the ion and electron temperatures are the same. The ion to electron mass ratio is reduced to $m_i/m_e = 400$. Each wave packet is initialized as the sum of 8 sinusoidal waves with their maximum at $X = 300$ for the first wave packet, and $X = 100$ for the second wave packet. The equations defining the waves polarisations are given in the appendix in (Mottez 2008). The first wave packet propagates downward (in the direction of decreasing values of X). The sinusoidal waves that compose the wave packet have the same amplitude, given by the wave magnetic field $\delta B = 0.05 \times B_0$. The waves have a right handed circular polarization. Their wavelengths are $\lambda = \lambda_0/m$ where $\lambda_0 = 409.6$ and m varies from 1 to 8. The phase velocities vary from 0.109 for the shortest wave to 0.046 for the longest. (The Alfvén velocity is $V_A = 0.04$.) The second wave packet propagates upward. Apart from its direction of propagation and location, its characteristics are the same.

The B_z component of the magnetic field is a proxy of the wave packets propagation. It is plotted as a function of X and time on Fig. 1. We can see that the two packets cross each other at time $t \sim 10^4$ and $X \sim 200$, and latter a times $t \sim 2.10^4$, $t \sim 3.10^4$ etc.

For the other simulations, a few parameters are varied. When a physical parameter is varied (for instance, a wave amplitude), the number is different. The parameters of these simulations are summarized in Table 1. We can notice that these simulations all involve the right-hand circularly polarized waves propagating in opposite directions, as in AWC009. We made the deliberate choice to concentrate on this subset of parameters because, as shown in (Mottez 2012a), it represent a favourable case for parallel to B_0 electric field, and because the RH waves are less dispersive than the LH ones. This make the physical interpretation of the simulation easier. Concerning dimensions, a 2D simulation was presented in (Mottez 2012a) with the same initial configuration as the 1D simulations. The plasma behaved exactly as in 1D simulations. This is why 2D simulations are not repeated in the present study.

The simulation AWC009 is based on a magnetic field $B_0 = 0.8$ that is five times smaller than those in (Mottez 2012a). This is a deliberate choice in order to check the robustness of APAWI relative to the ambient magnetic field amplitude. Nevertheless, we can notice that the plasma β (see Table 1) is typical of a highly magnetized plasma ($\beta \ll 1$). In the simulations with $B_0 = 4$, $\beta < m_e/m_i = 10^{-2}$ is typical of the largest part of acceleration region of the auroral zone. To illustrate more precisely the physical

name	B_0	Δt	$ \delta B/B_0 $	β	λ	
AWC001	0.8	0.2	0.02	$1.6 \cdot 10^{-2}$	204.8	unperturbed f_e and f_i
AWC002	0.8	0.2	0.2	$1.6 \cdot 10^{-2}$	204.8	weak modulation of f_e and f_i
AWC003	0.8	0.2	0.02	$1.6 \cdot 10^{-2}$	51.2-409.	weak modulation of f_e and f_i
AWC004	0.8	0.1	0.04	$1.6 \cdot 10^{-2}$	204.8	modulation of f_e and f_i
AWC005	0.8	0.1	0.024	$1.6 \cdot 10^{-2}$	51.2-409.	modulation of f_e and f_i
AWC006	2.0	0.05	0.10	$0.5 \cdot 10^{-2}$	204.8	modulation of f_e and f_i
AWC007	2.0	0.05	0.06	$0.5 \cdot 10^{-2}$	51.2-409.	f_e vortices, f_i vortices & beams
AWC008	0.8	0.1	0.10	$1.6 \cdot 10^{-2}$	204.8	electron cavities, ion beams
AWC009	0.8	0.1	0.05	$1.6 \cdot 10^{-2}$	51.2-409.	electron cavities & bumps, ion beams.
AWC014	4.0	0.025	0.20	$0.25 \cdot 10^{-2}$	204.8	modulation of f_e , ion beams
AWC015	4.0	0.025	0.12	$0.25 \cdot 10^{-2}$	51.2-409.	electron vortices & cavities bulk ion acceleration & beam
AWC016	4.0	0.025	0.05	$0.25 \cdot 10^{-2}$	204.8	f_e and f_i hardly not modulated
AWC017	4.0	0.025	0.02	$0.25 \cdot 10^{-2}$	51.2-409.	f_e and f_i hardly not modulated
AWC019	4.0	0.025	0.06	$0.25 \cdot 10^{-2}$	51.2-409.	strong electron cavities, ion beams

TABLE 1. Varied simulation parameters and comments on the evolution of the particle distribution functions $f_e(X, V_x)$ (electrons) and $f_i(X, V_x)$ (ions). The wave amplitudes $\delta B/B_0$ and the range of wavelengths λ are the same for the two waves/wave packets; they are not repeated in the table.

context, let us notice that the "classical" theories of acceleration by oblique Alfvén waves (therefore not APAWI) involve inertial AW in this range of altitudes (Thompson & Lysak 1996; Lysak & Song 2003b). With $B_0 = 2$ or 0.8 , $m_e/m_i < \beta \ll 1$ is representative of the upper part of the auroral zone where acceleration by oblique AW is caused by kinetic AW (Hasegawa & Mima 1978). Such low values of the plasma β can also be relevant for the study of the inner solar corona.

Considering $\beta \ll 1$ reinforces the choice of simulations with right-hand (RH) circularly polarized waves rather than left-hand (LH) waves, because in this regime, as shown by Buti *et al.* (2000), LH Alfvén wave packets are unstable to collapse or with possible change of polarization, while RH Alfvén wave packets are stable. Such phenomenon would make the interpretation of the simulations more difficult relatively to APAWI.

We can notice that because of the limited size of the simulation domain, and hence of the wavelengths, the wave packet is dispersive. The frequencies corresponding to the small wavelengths is higher than the ion gyro-period ($T_{ci}\omega_{pe} = 3141$), placing those waves nearly in the domain of electromagnetic whistler waves rather than MHD Alfvén waves. Nevertheless, these waves are on the same branch of the linear dispersion relation, and they are both observed in the auroral zone and many other regions of the magnetosphere.

3. Properties of the electromagnetic field

We consider two sinusoidal waves labelled 1 and 2, and their associated magnetic field,

$$\begin{aligned}
 B_X &= B_0 \\
 B_Y &= B_{1Y} \cos(\omega t - kX + \phi_{B_{1Y}}) + B_{2Y} \cos(\omega t + kX + \phi_{B_{2Y}}) \\
 B_Z &= B_{1Z} \cos(\omega t - kX + \phi_{B_{1Z}}) + B_{2Z} \cos(\omega t + kX + \phi_{B_{2Z}})
 \end{aligned}
 \tag{3.1}$$

We write the phase relations in the form

$$\phi_{B_{1Z}} = \phi_{B_{1Y}} + n_1\pi/2
 \tag{3.2}$$

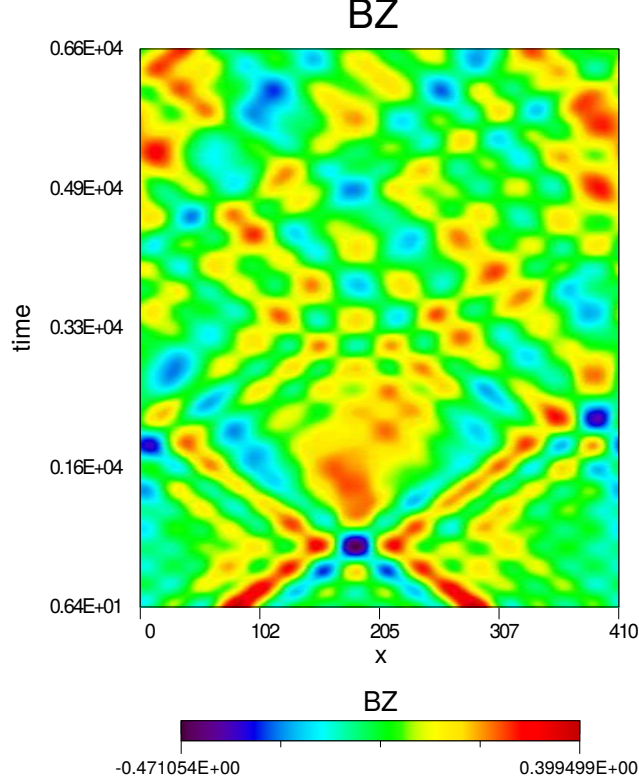


FIGURE 1. AWC009. Temporal stack plot of the transverse magnetic field $B_Z(X, t)$.

with $n_1 = \pm 2$ for linear polarization, $n_1 = +1$ for right-handed waves, $n_1 = -1$ for left-handed waves. With circularly polarised waves, $B_{1Y} = B_{1Z}$, $B_{2Y} = B_{2Z}$ and we write simply B_1 and B_2 . Because the magnetic field modulus B is required in the next section to compute the dynamics of the particles, we develop it here,

$$\begin{aligned}
 B^2 = & B_0^2 + B_{1Y}^2 \cos^2(\omega t - kX + \phi_{B_{1Y}}) \\
 & + B_{2Y}^2 \cos^2(\omega t + kX + \phi_{B_{2Y}}) \\
 & + B_{1Z}^2 \cos^2(\omega t - kX + \phi_{B_{1Y}} + n_1 \frac{\pi}{2}) \\
 & + B_{2Z}^2 \cos^2(\omega t + kX + \phi_{B_{2Y}} + n_2 \frac{\pi}{2}) \\
 & + B_{1Y} B_{2Y} [\cos(2\omega t + \phi_+) + \cos(2kX + \phi_-)] \\
 & + B_{1Z} B_{2Z} \cos(2\omega t + \phi_+ + (n_1 + n_2) \frac{\pi}{2}) \\
 & + B_{1Z} B_{2Z} \cos(2kX + \phi_- + (n_2 - n_1) \frac{\pi}{2}),
 \end{aligned} \tag{3.3}$$

where $\phi_- = \phi_{B_{2Y}} - \phi_{B_{1Y}}$ and $\phi_+ = \phi_{B_{2Y}} + \phi_{B_{1Y}}$. We find the well known property that a single wave with circular polarisation has a uniform magnetic field amplitude. With two waves with the same circular polarisation ($n_1 = n_2$), the modulus is purely space dependent,

$$B^2 = B_0^2 + B_1^2 + B_2^2 + 2B_1 B_2 \cos(2kX + \phi_-). \tag{3.4}$$

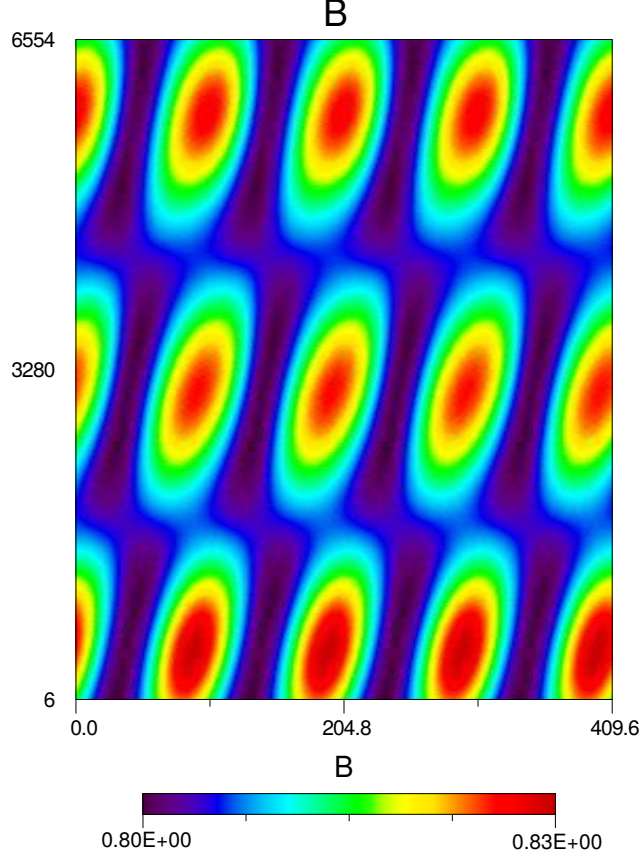


FIGURE 2. AWC008. Temporal stack plot of the magnetic field amplitude $B(X, t)$.

Fig 2 shows the stack plot of the magnetic field modulus in simulation AWC008. We can see that unlike Eq. (3.4), it is not purely space dependent. This may be caused by an imperfect initialisation of the waves polarisation. Nevertheless, it is not oscillating either and the regions of maximas and of minimas of B are static. Two waves with opposite circular polarisation ($n_1 = -n_2$) have a purely time dependent modulus,

$$B^2 = B_0^2 + B_1^2 + B_2^2 + 2B_1B_2 \cos(2\omega t + \phi_+). \quad (3.5)$$

The ability of the two waves to create an electric field with a component E_X that is parallel to the average magnetic field was investigated in (Mottez 2012a). This property holds with the simulations made since then. But it was found in the theoretical derivation in (Mottez 2012a) that some terms appeared that could not be seen in the numerical simulations. They were self-coupling terms in the sense that they involved only one wave. A new derivation of E_X is presented in appendix A, where the constraint brought by the Ampere-Faraday law is taken into account. We find a parallel electric field E_X that contains only the terms seen in the numerical simulations, and not the self-coupling ones,

$$\begin{aligned} kB_0 E_X / \omega = & \quad (3.6) \\ & -B_{1Z}B_{2Y} [\cos(2kX + \phi_- - \frac{n_1\pi}{2}) + \cos(2\omega t + \phi_+ + \frac{n_1\pi}{2})] \\ & + B_{1Y}B_{2Z} [\cos(2kX + \phi_- + \frac{n_2\pi}{2}) + \cos(2\omega t + \phi_+ + \frac{n_2\pi}{2})]. \end{aligned}$$

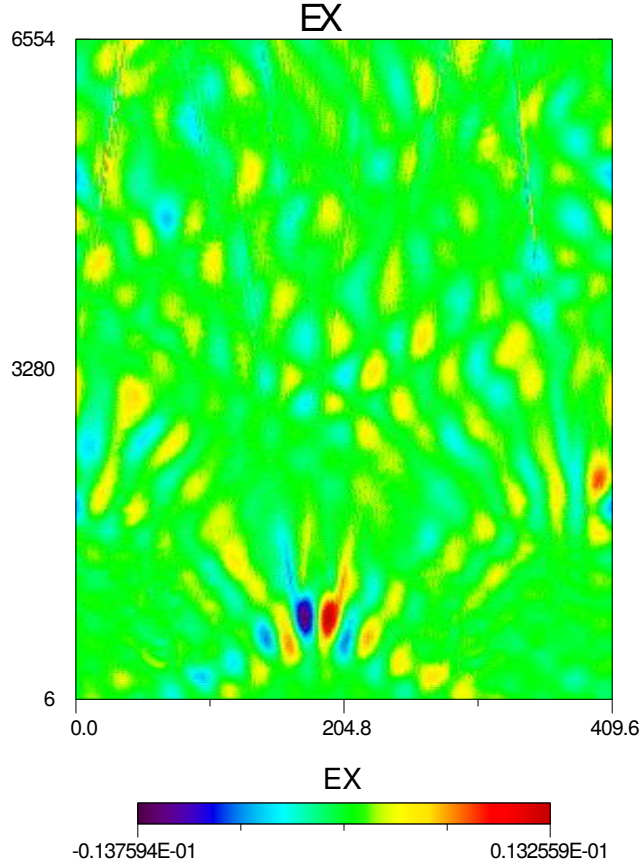


FIGURE 3. AWC009. Temporal stack plot of the electric field $E_X(X, t)$ parallel to \vec{B}_0 . In order to remove plasma oscillations near the plasma frequency, the signal was filtered with a first order low-pass filter (cut-off frequency $0.5\omega_{pe}$).

When the two waves are linearly polarized and coplanar, $E_X = 0$. When the two waves are linearly polarized and orthogonal, for instance $\phi_{B_{1z}} = \phi_{B_{2y}} = 0$, $E_X = 2B_{1Y}B_{2Z} \cos(\omega t - kX + \phi_{B_{1Y}}) \cos(\omega t + kX + \phi_{B_{2Z}})$.

When the two waves are circularly polarized of opposite direction (left and right-handed), E_X is purely temporal of period 2ω , there is no spatial dependence.

When the two waves are circularly polarized, with the same polarization ($n_1 = n_2$) E_X is purely spatial of wave vector $2k$, there is no temporal dependence.

$$kB_0E_X/\omega = 2B_1B_2 \cos(2kX + \phi_- + n\frac{\pi}{2}). \quad (3.7)$$

Eq. (3.6) fits the electric field E_X found with the simulations presented in (Mottez 2012a) as well as the simulations attached to the present work. This point was analysed in details in (Mottez 2012a) and we do not repeat the analysis here.

It is interesting to see that B and E_X are purely space dependent under the same circumstances (two waves with the same circular polarisation) and purely time dependent as well (two waves with opposite circular polarisations).

This result, set analytically for two sinusoidal waves holds for two wave packets. The stack plot of E_X is shown in Fig. 3 for simulation AWC009. We can see the setting of a

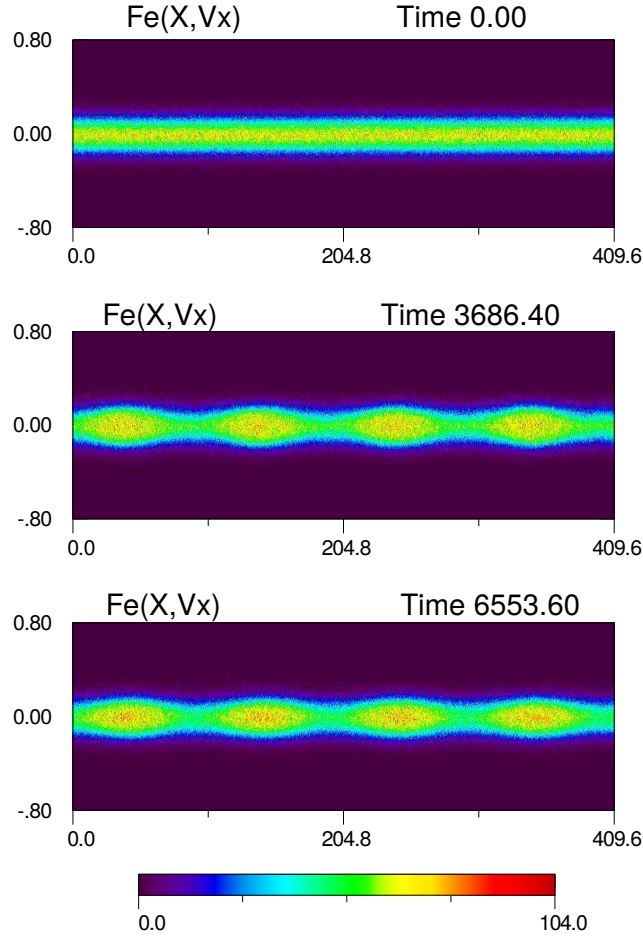


FIGURE 4. AWC008. Snapshots of the electron distribution function as a function of X and the velocity V_x parallel to the local magnetic field \vec{B} .

finite E_X at the places and times that correspond to wave packets crossings. This electric field is stationary... as long as the crossing lasts. Later, E_X vanishes.

4. Particle acceleration along the mean magnetic field direction

Let us consider a particle of velocity $\vec{V} = \vec{V}_x + \vec{V}_\perp$ where the indexes \parallel and \perp are relative to the local magnetic field direction. We note $\vec{b} = \vec{B}/B$. Considering the guiding centre theory of motion, the motion along the magnetic field line is governed by the parallel electric field E_x and the parallel gradient of the magnetic field modulus

$$\frac{dV_x}{dt} = \frac{q}{m} E_x - \frac{\mu}{m} \nabla_\parallel B. \quad (4.1)$$

We have postulated, and seen in the numerical simulations that $E_x = 0$ (only E_X is finite), then

$$\frac{dV_x}{dt} = -\frac{\mu}{m} \frac{dB}{dx} = -\frac{\mu}{m} \frac{dB}{dX}, \quad (4.2)$$

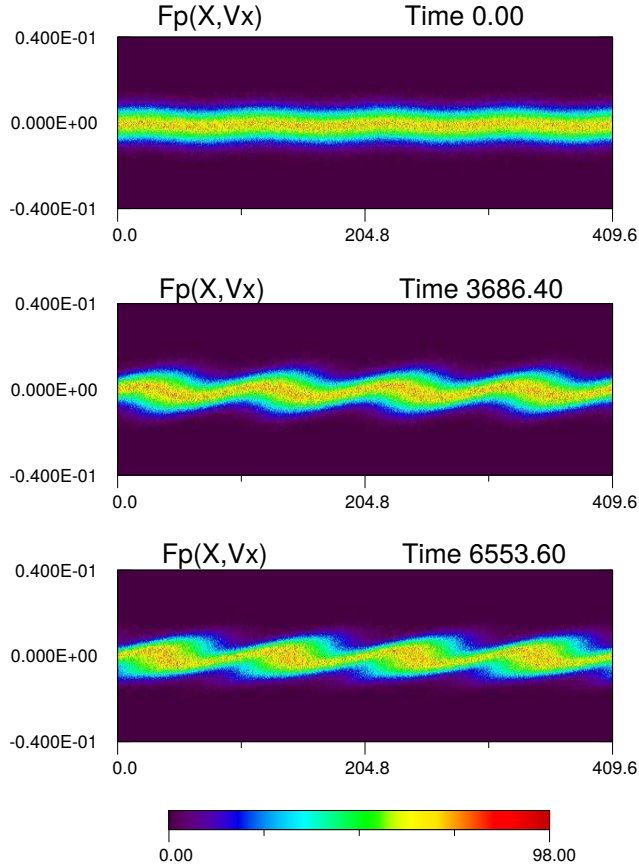


FIGURE 5. AWC008. Snapshots of the ion distribution function as a function of X and the velocity V_x parallel to the local magnetic field \vec{B} .

the second equality being correct when the wave magnetic perturbation is small compared to B_0 . This acceleration scales as

$$\frac{dV_x}{dt} \sim \frac{T}{m} \frac{1}{B} \frac{dB}{dX}, \quad (4.3)$$

and because the temperature is the same (in the simulations) for the ions and for the electrons, and because the electrons are lighter, this acceleration is dominant for the electrons.

We can see that when the two waves have opposite circular polarisation, B is purely time dependent. Therefore, there is no gradient, and no parallel particle acceleration at all. This case was tested with the simulation AWC011 in (Mottez 2012a). The electric field in AWC011 was purely time dependent, in accordance with Eq. (3.6). The electron and ion distributions $f_e(x, V_x)$ and $f_i(x, V_x)$ (not shown on a figure) remained exactly identical to their initial values, in accordance with the fact established here that there is no force acting on the parallel velocity.

From Eq. (3.4), two opposite sinusoidal waves with the same circular polarisation make regions of acceleration with a fixed position and no time dependence. This is actually what is seen in the simulations. Figs. 4 and 5, show the electron and ion distribution functions as functions of X and V_x from the simulation AWC008. We can see a periodic

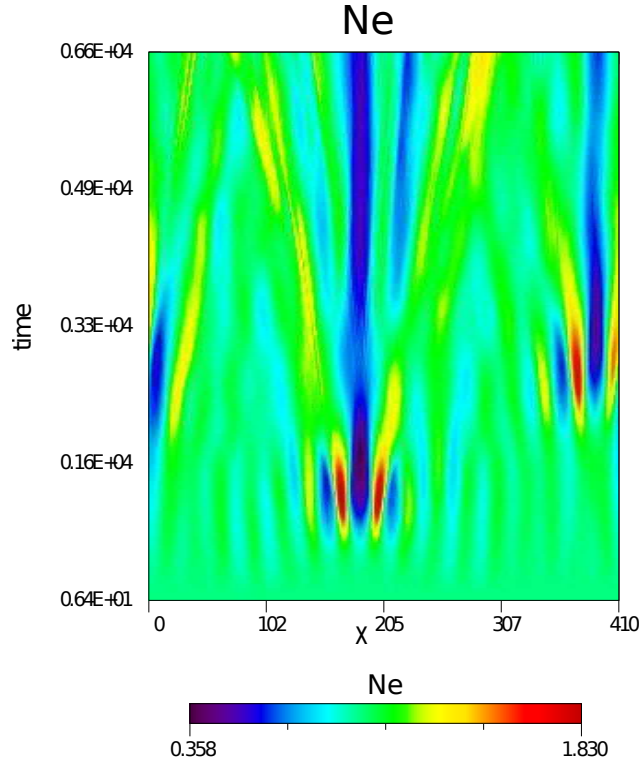


FIGURE 6. AWC009. Temporal stack plot of the electron density $N_e(X, t)$.

modulation of the electron and ion densities with a mode number $m=4$ that is twice those of the two sinusoidal Alfvén waves. Concerning wave packets interactions, an example is given in Fig. 6 that show the stack plot of the electron density for the simulation ACW009. We can notice that an important effect of the gradient of B is the creation of a zone of electron depletion. This depletion is created at the two wave packets crossing, but, contrarily to the E_X electric field, it remains after the wave packets crossings. The electron depletion can be seen as well on Figs. 7, 8 that represent the electron distribution as functions of X and V_X and of X and V_x . The fact of using V_x or V_X does not change the general aspect of the figures. This means that what is seen of these distribution is not a mere effect of projection (on the local or the average magnetic fields) but a real structure. Fig. 9 shows the ion distribution as a function of X and V_x . We can see ion beams initiated around the positions of the wave packets crossings. Figure 9 is more dramatic than Fig. 5 simply because the wave packets in AWC009 have a larger amplitude than the sinusoidal waves in AWC008.

Does the electric field play a role in the acceleration process in the perpendicular velocity \vec{V}_\perp ? Would a projection of this velocity along the X axis imply acceleration in that direction? Because the geometry of the problem is 1D, there is no perpendicular gradient of B . Because the magnetic perturbation caused by the waves is small compared to B_0 the magnetic field line curvature is negligible. The perpendicular velocity \vec{V}_\perp is therefore reduced to the sum of the cross field drift and of the polarisation drift, and its

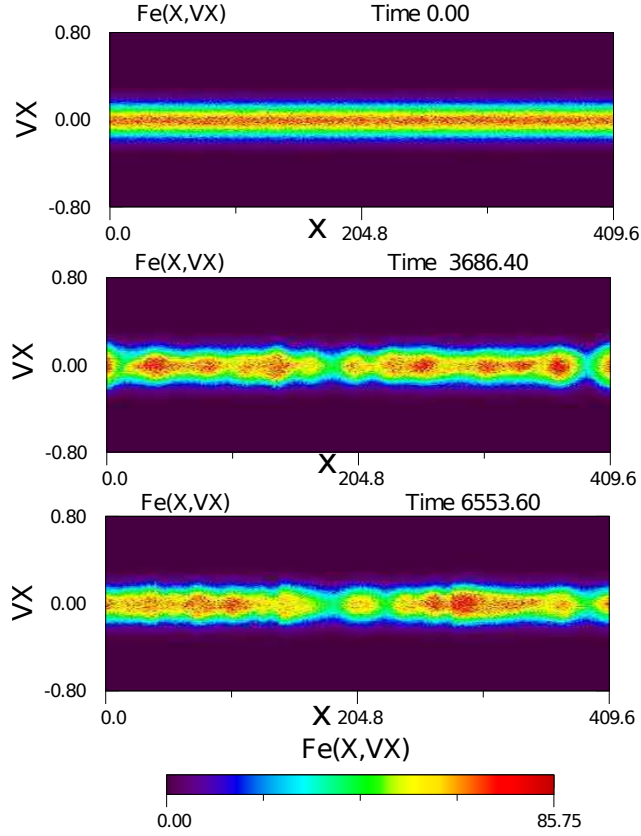


FIGURE 7. AWC009. Snapshots of the electron distribution function as a function of X and of the velocity V_X parallel to the *mean magnetic field* \vec{B}_0 .

projection along the ambient magnetic field direction \vec{e}_X is

$$\vec{V}_\perp \cdot \vec{e}_X = \frac{(\vec{e}_X \times \vec{E}) \cdot \vec{B}}{B^2} + \frac{m}{qB^2} \frac{d(\vec{E} \cdot \vec{e}_X)}{dt}. \quad (4.4)$$

For two sinusoidal waves with the same circular polarisation,

$$\vec{V}_\perp \cdot \vec{e}_X = \frac{\omega}{kB_0^2} [B_1^2 - B_2^2 - 4B_1B_2 \frac{mkV_X}{qB_0} \sin(2kX + \phi_- + n\frac{\pi}{2})]. \quad (4.5)$$

The two first terms come from the cross fields drift, the third from the polarisation drift. The space dependent part of this velocity scales as

$$\vec{V}_\perp \cdot \vec{e}_X \sim -4V_X \frac{B_1B_2}{B_0^2} \frac{\omega}{\omega_c} \cos(2kX + \phi_-); \quad (4.6)$$

it is dominant for the ions. In conclusion, with two circular waves with the same polarisation, a sinusoidal and purely space dependent ion velocity perturbation is set. It is caused by the projection E_X of the electric field on the average magnetic field direction. The electrons are accelerated by a magnetic gradient force that also depends on space, and not on time. We can compare the ion and the electron accelerations. The ion acceleration is the time derivative of the expression in Eq. (4.5). We find that the ratio of the electron

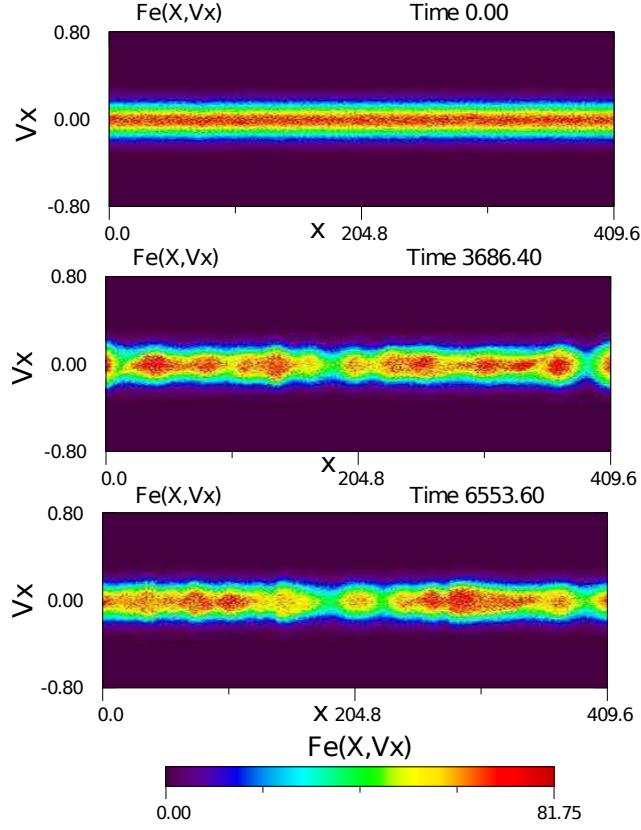


FIGURE 8. AWC009. Snapshots of the electron distribution function as a function of X and the velocity V_x parallel to the *local magnetic field* \vec{B} .

to ion accelerations scales as

$$\frac{a_e}{a_i} \sim \frac{1}{4} \frac{T_e}{T_i} \frac{m_i}{m_e} \frac{\omega_{ci}}{\omega} \quad (4.7)$$

where we have set $V_X \sim v_{ti}$, $\mu/m \sim v_{te}^2/B_0$, and ω_{ci} is the ion cyclotron frequency. When the electron and ion temperatures are similar and $\omega/\omega_{ci} > 0.1$, the electron acceleration is much higher than the ion acceleration.

Therefore, the electrons are first accelerated. The ions do not follow and a charge separation parallel electric field is set. This electric field may accelerate the ions more efficiently than the polarisation drift would do, and cause the ion beams than we can see on Fig. 9 and (less) on Fig. 5.

The last column of Table 1 indicate briefly the behaviour of the particles distribution function for each numerical simulation. We can see that the distribution functions become easily modulated. These modulation result in density modulations and plasma cavities of moderate depth. Deep cavities, electron vortices and ion beam appear for higher wave amplitudes.

5. Observational characteristics of APAWI

The APAWI process requires two counter-propagating waves of the same wavelength. Actually, it is not precisely needed that they are Alfvén waves, but it is necessary that,

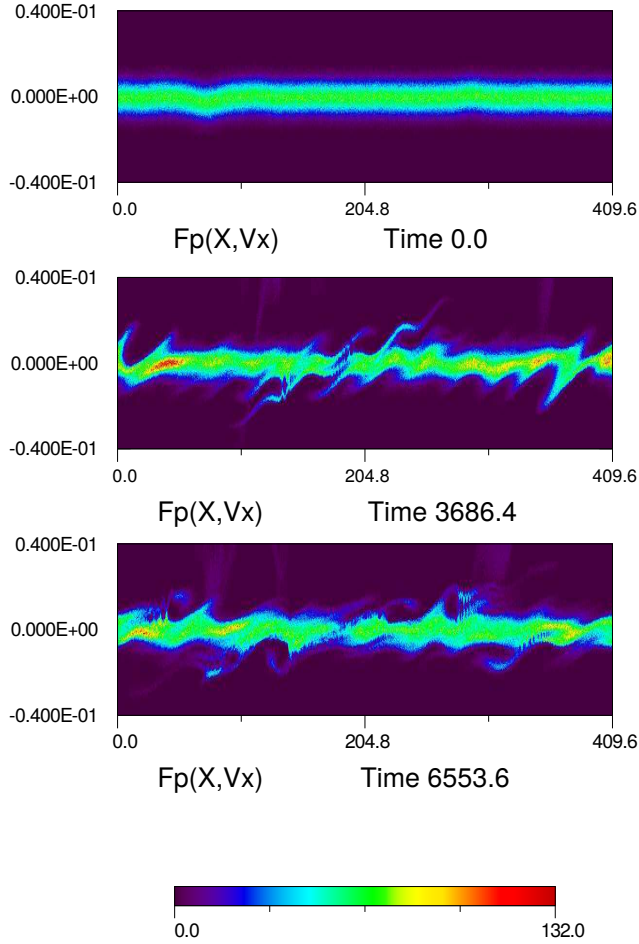


FIGURE 9. AWC009. Snapshots of the ion distribution function as a function of X and the velocity V_x parallel to the *local magnetic field* \vec{B} .

like MHD and ideal Hall MHD waves, the local electric field is perpendicular to the local magnetic field.

From an observational point of view, we can make the distinction between the interaction of two wave packets and a standing wave.

When two wave packets interfere, the area (along the magnetic field lines) where E_X and ∇B fields are finite is comparable to the size of the wave packets. The duration of its occurrence is the duration of the superposition of the two wave packets. Let us assume that the wave packets have a propagation velocity V_{wp} and a typical size L_{wp} , then, the non-oscillatory electric field last for a time lapse $\tau \sim L_{wp}/V_{wp}$. This is the same time during which an isolated (of both) wave packet(s) is seen from a fixed position.

For instance, in the Earth Auroral zone, a first Alfvén wave packet coming from the magnetotail can be reflected on the ionosphere. A second wave packet of comparable size can arrive later and cross the reflected part of the first packet. Louarn *et al.* (1994) observed Alfvén wave packets in the low altitude auroral zone (~ 1000 km above ground), during about 10 ms. If two wave packets like those cross each other, then, the non-oscillating electric field E_X and the non-oscillating magnetic gradient would also have a

duration of approximately 10 ms. This would correspond to the duration of the acceleration process.

A standing wave can be considered as the superposition of two sinusoidal counter-propagating waves. In that case, the region where non oscillatory E_X and ∇B fields are finite extends over a significant fraction of the trapped wavelength (about 25%). The simulations show that these regions are associated with a deep plasma density depletion. The computation of the magnetic field modulus B in Eq. (3.4) when the waves have the same polarisation (optimal condition for acceleration) show that it has a purely spatial dependence, with a scale-length twice smaller than those of the standing waves. The APAWI regions associated with trapped waves exist as long as the wave trapping occurs. This can be a much longer duration than with the interaction of two wave packets. Because of this longer duration, it may be more probable to observe APAWI associated with wave trapping than to wave packets interaction.

6. APAWI in space plasmas

APAWI might be efficient when acceleration occurs along a closed magnetic field loop provided that parallel Alfvén waves propagate along it. Melrose & Wheatland (2013) have discussed the role of a dense network of striated Alfvén waves in closed loops in the solar corona, and their link with particle acceleration. They suggest that the acceleration comes from Alfvén waves inertial effects (implying oblique propagation). No explicit explanation for the oblique (quasi-perpendicular) propagation of the Alfvén waves is given (for the phase velocity), therefore, we may as well imagine phase velocities parallel to the ambient magnetic field. We suggest that in the context described by Melrose & Wheatland (2013), Alfvén waves with $k = k_{\parallel}$ could play the same role as the oblique inertial Alfvén waves relative to transport and acceleration. In the model in Melrose & Wheatland (2013), the Alfvén waves transport energy from the point where they are generated toward the point where they accelerate particles and dissipate. If we suppose that coronal loops support wave packets going down from the generator region and others going up after reflection above the photosphere, APAWI would occur at the place where they meet.

A recent example given by Yuan & Zong (2013), illustrate the possibility of APAWI in the Earth radiation belts. The authors identified eight events with double-belt structure associated with magnetic storms, based on the SAMPEX data sets. All double-belt structure events in the outer radiation belt are found during the recovery phase of a magnetic storm. The authors suggest that the plasmopause and the strong wave-particle interactions with VLF and ULF waves near it play an important role in the development of the double-belt structures. Actually, the radiation belts are, like the loops of the sun corona, regions of closed magnetic field lines where trapped ULF can take place. These trapped waves could be intensified during the preconditions identified by Yuan & Zong (2013) and cause APAWI. Then, APAWI could be a cause of the energetic particles double-belt structure. However, it is not proved yet that APAWI can operate in this range of energies; this question is left for a further study.

Contrary to coronal loops and radiation belts, the Earth auroral zone contains open magnetic field lines. Nevertheless, the role played by Alfvén waves in auroral acceleration is of paramount importance. Alfvén waves are very often observed in the auroral zone (Stasiewicz *et al.* 2000). They take the form of isolated wave packets carrying a significant amount of Poynting flux (Volwerk *et al.* 1996), as well as Alfvén waves trapped in an auroral zone cavity called the ionospheric Alfvén resonator (Chaston *et al.* 2002; Lysak & Song 2003a). Both trapped waves and wave packets are associated with fluxes

of accelerated particles. Lund (2010) have studied the cut-off of turbulent Alfvén wave spectra in the Earth auroral zone with FAST data. The authors have found cuts-off at the electron cyclotron scale, and at the electron inertial lengths. These cuts-off are the signatures of dissipation by perpendicular ion heating and by parallel electron acceleration. This conforms to the picture of acceleration by quasi-perpendicular Alfvén waves associated with electron inertial and kinetic effects (Lysak 1991; Thompson & Lysak 1996; Watt & Rankin 2010; Mottez & Génot 2011). But Lund (2010) also noticed that there is no evidence of damping at the ion inertial length. This result implies that there is no power in the quasi-parallel shear Alfvén mode at FAST altitudes above a few Hz. These waves are known to be present at higher altitudes. According to Lund (2010), this suggest some attenuation mechanism at a plasma frame frequency of ~ 1 Hz, that is, just above the cavity modes frequencies of the ionospheric Alfvén resonator (Lysak 1991). We suggest that the absorption of the quasi-parallel Alfvén waves above ~ 1 Hz results from APAWI associated with the trapped Alfvén waves in the ionospheric resonator.

APAWI can also be an explanation to the formation of deep plasma cavities in the Earth auroral zone. These cavities where plasma density abruptly drops to less than 50% of the ambient plasma density are ubiquitous in the auroral zone. They are associated with auroral acceleration processes and auroral kilometric radiation (Persoon *et al.* 1988; Hilgers 1992; Mäkelä *et al.* 1998). Theories concerning their origin involve inertial Alfvén waves and/or ponderomotive forces (Singh 1992; Shukla & Stenflo 1999) or transverse heating mechanism Singh (1994). We can see that APAWI is an alternative model for cavity formation that arises naturally when one considers the existence of trapped Alfvén waves in the ionospheric resonator.

7. Discussion and conclusion

The APAWI process is characterised by the following properties: The crossing of up-going and down-going parallel propagating Alfvén waves with the same circular polarisation generates time independent electric fields and magnetic modulus gradients along the direction of propagation of the waves. Both electric field and magnetic gradient amplitudes are quadratic non-linear effects; there is no critical threshold. They cause significant modulation of the plasma density. They cause particle acceleration.

Can APAWI be investigated with MHD ? The parallel electric field could be evidenced in MHD with the correct polarisation, although the electric field is rarely investigated with MHD codes. It is not specific to the PIC simulations nor to any kind of Maxwell-Vlasov analysis. But the consequences of this electric field on the plasma cannot be put clearly in evidence with MHD equations, because as shown on Fig. 9, it does not act in a simple way on the mean velocity or the plasma temperature. The use of a plasma kinetic approach is then required, unless a proxy is found to characterise the effect of the parallel non-oscillating electric field with MHD or any other kind of fluid plasma equations.

Many simulations have been devoted to the dynamics of incoming Alfvén waves and their reflected counterpart on the ionosphere, especially in the context of the ionospheric Alfvénic resonator (Lysak 1991; Thompson & Lysak 1996; Watt & Rankin 2010). In these situations, there are two Alfvén waves (whatever in the form of wave packets or of standing waves) with the same polarisation and opposite directions. Why was APAWI not seen in these simulations ? Very often, simulations for Alfvén waves derive the magnetic perturbation from a vector potential $A_{\parallel}(X, Z, t)$ (parallel to B_0). This implies that $\delta\vec{B}$ is perpendicular to \vec{B}_0 that is compatible with the input of the theory presented in this paper. But it also means that the electric field derived from the vector potential

is perpendicular to \vec{B}_0 and it does not fit the requirement that \vec{E} is perpendicular to $\vec{B} = \vec{B}_0 + \delta\vec{B}$. One of the basic principles of APAWI is forbidden by the use of $A_{\parallel}(X, Z, t)$. It is also important that the Alfvén wave polarisation is compatible with the presence of circularly polarised waves.

Of course, APAWI is not the only one acceleration process at work in space plasmas. For instance, the above cited work in Lund (2010) also makes a large room for other Alfvénic acceleration processes. In order to avoid confusions, we review shortly what APAWI is not.

Ponderomotive force associated with Alfvén waves have been investigated by Singh (1994); Sharma & Singh (2009). It was shown that it leads to the creation of density cavities. But ponderomotive force derives from the spatial modulation of a wave envelope. It acts therefore at the same scale as the envelope and not at the smaller scale defined by the wavelength. In APAWI, as we have seen with the theoretical treatment of two waves interaction, the acceleration structures scale as the wavelength, and they do not involve any modulation of the waves amplitudes. Therefore APAWI is not acceleration by a ponderomotive force. This is an alternative process acting on a smaller scale length.

Because the cavities created by the APAWI are smaller than the wavelengths, the waves that caused these cavities cannot be trapped in it. But it is not excluded that waves with smaller wavelengths then become trapped in these cavities formed by APAWI. Then, the observational data may become more complex, making its analysis more difficult.

Contrary to acceleration by inertial of kinetic Alfvén waves, no oblique propagation is required, and instead of $k_{\perp}c/\omega_{pe} \sim 1$ or $k_{\perp}\rho_i \sim 1$, it is simply required that $k_{\perp} = 0$. There is no specific requirement on the parallel wavelength.

The acceleration by an Alfvén wave with a velocity close to the thermal electron velocity has been investigated by Watt & Rankin (2008). This involves Landau resonance for electrons in the wave fields. With APAWI, the acceleration region is static or quasi-static. No resonance effect that would select the range of initial energies of the accelerated particles is involved. This is not resonant acceleration.

An Alfvén wave in parallel propagation over plasma density cavities soon develop small transverse scales, parallel electric fields (Génot *et al.* 1999) and causes plasma acceleration (Génot *et al.* 2001). With APAWI, the density cavities are a result of the process and not an initial ingredient. APAWI can work in an initially uniform plasma.

The decay of Alfvén waves into a daughter Alfvén wave and an acoustic-like wave can trigger the formation of ion beams (Matteini *et al.* 2010). Modulational instabilities can result as well in ion beam acceleration (Araneda *et al.* 2008). Is ion acceleration seen with APAWI really the result of the process described in section 4, or the result of an unnoticed AW decay or modulational instability? Figure 5 shows that the modulation of the ion distribution function has a wave number $m = 4$ for initial Alfvén wave numbers $m_1 = m_2 = 2$. This is consistent with the multiplication by two of the initial wave vector seen, for instance, in Eq. (3.4). This is not compatible with the slightly more complex wave number ratios involved with parametric instabilities. Therefore, we are tempted to conclude that ion acceleration is directly related to APAWI, and not to a parametric instability.

Therefore we can conclude that APAWI does not involve ponderomotive force, inertial or kinetic Alfvén waves, resonant acceleration or propagation effects on a non-uniform plasma, or parametric instabilities. Of course, APAWI can act simultaneously with one of these and the consequences of APAWI can be similar to those of other acceleration mechanisms. For instance, like ponderomotive forces, APAWI causes deep plasma density depletions; like the parametric instabilities, it can cause ion beams.

In conclusion of this paper, acceleration by parallel Alfvén waves interaction (APAWI)

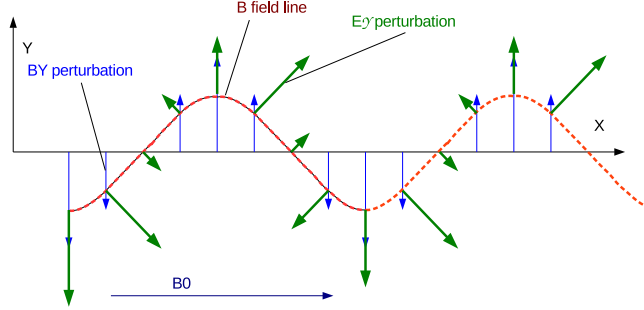


FIGURE 10. Schematic explanation of the parallel electric field E_X parallel to the average magnetic field \vec{B}_0 .

is a new method of accelerating plasma particles with Alfvén waves. The existence of APAWI does not rule out the relevance of other Alfvénic processes, but it enlarges the range of plasma parameters and waves polarisations that make possible plasma acceleration by Alfvén waves. More specifically, it is the only acceleration process known up to now that involves only parallel Alfvén waves and an initially homogeneous plasma. APAWI may be relevant in a very large number of space plasma contexts, including planetary magnetospheres and magnetic loops in the Sun corona. It is a very efficient way of creating plasma cavities such as those observed in the Earth auroral zone.

Appendix A. Parallel electric field

We define the two angles θ_Y and θ_Z by the relations

$$\frac{B_Y}{B_0} = \tan \theta_Y \text{ and } \frac{B_Z}{B_0} = \tan \theta_Z. \quad (\text{A } 1)$$

Because we consider that the MHD waves amplitude is low relative to the ambient magnetic field B_0 , we consider that these angles are small.

The ideal Ohm's law, used for MHD waves, implies that the electric field and the magnetic field are orthogonal. This holds when the Ohm's law includes the Hall effect,

$$\vec{E} + \vec{v} \times \vec{B} = \frac{\vec{J}}{qn} \times \vec{B}. \quad (\text{A } 2)$$

The situation is schematically displayed on Fig. 10 where the electric field is represented by thick arrows (green in the electronic version). The electric field is perpendicular to the (dashed/red) magnetic field line, and the magnetic perturbation vectors (thin blue arrows) are perpendicular to the X direction. In terms of vector components, $E_x = 0$, but we can see that E_X (projection of the electric field along the *average* magnetic field \vec{B}_0) can be finite. The local coordinate system (x, y, z) is based on the direction of the magnetic field, with \vec{e}_x parallel to \vec{B}_0 . The magnetic field lines are defined by,

$$\frac{dX}{B_0} = \frac{dY}{B_Y} = \frac{dZ}{B_Z}. \quad (\text{A } 3)$$

The following computation is based on the hypothesis of small angles $\theta_Y \ll 1$ and

$\theta_Z \ll 1$. It is based on first order developments relative to these angles. Then,

$$\frac{dY}{dX} = \frac{B_Y}{B_0} = \tan \theta_Y = \theta_Y \quad \text{and} \quad \frac{dZ}{dX} = \frac{B_Z}{B_0} = \tan \theta_Z = \theta_Z. \quad (\text{A } 4)$$

Making projections,

$$E_X = -E_y \sin \theta_Y - E_z \sin \theta_Z \sim -E_y \frac{B_Y}{B_0} - E_z \frac{B_Z}{B_0}. \quad (\text{A } 5)$$

With two sinusoidal waves labelled 1 and 2,

$$\begin{aligned} E_x &= 0, \\ E_y &= E_{1y} \cos(\omega t - kX + \phi_{E_{1y}}) + E_{2y} \cos(\omega t + kX + \phi_{E_{2y}}), \\ E_z &= E_{1z} \cos(\omega t - kX + \phi_{E_{1z}}) + E_{2z} \cos(\omega t + kX + \phi_{E_{2z}}). \end{aligned} \quad (\text{A } 6)$$

In addition to the computation presented in (Mottez 2012a), we take into account the constraint raised by the Faraday equation

$$\nabla \times \vec{E} = -\frac{\partial \vec{B}}{\partial t}. \quad (\text{A } 7)$$

At first order in θ_Y and θ_Z ,

$$\begin{aligned} \vec{e}_y &= \vec{e}_{\bar{Y}} - \theta_Y \vec{e}_{\bar{X}}, \quad \vec{e}_z = \vec{e}_{\bar{Z}} - \theta_Z \vec{e}_{\bar{X}} \\ \vec{e}_x &= \theta_Y \vec{e}_{\bar{Y}} + \theta_Z \vec{e}_{\bar{Z}} + \vec{e}_{\bar{X}}. \end{aligned} \quad (\text{A } 8)$$

Reciprocally,

$$\begin{aligned} \vec{e}_{\bar{Y}} &= \vec{e}_y + \theta_Y \vec{e}_x, \quad \vec{e}_{\bar{Z}} = \vec{e}_z + \theta_Z \vec{e}_x \\ \vec{e}_{\bar{X}} &= -\theta_Y \vec{e}_y - \theta_Z \vec{e}_z + \vec{e}_x. \end{aligned} \quad (\text{A } 9)$$

The above expression of $\vec{e}_{\bar{X}}$ proves the validity of Eq. (A 5). Because the electromagnetic field depends on X , the Faraday law is written in the $(\vec{e}_{\bar{X}}, \vec{e}_{\bar{Y}}, \vec{e}_{\bar{Z}})$ basis,

$$\frac{\partial B_Y}{\partial t} = \frac{\partial E_Z}{\partial X} \quad \text{and} \quad \frac{\partial B_Z}{\partial t} = -\frac{\partial E_Y}{\partial X} \quad \text{and} \quad \frac{\partial B_X}{\partial t} = 0. \quad (\text{A } 10)$$

To the first order in θ_Y and θ_Z ,

$$E_Y = \vec{E} \cdot \vec{e}_{\bar{Y}} = E_y \quad \text{and} \quad E_Z = \vec{E} \cdot \vec{e}_{\bar{Z}} = E_z. \quad (\text{A } 11)$$

Therefore,

$$\frac{\partial B_Y}{\partial t} = \frac{\partial E_z}{\partial X} \quad \text{and} \quad \frac{\partial B_Z}{\partial t} = -\frac{\partial E_y}{\partial X} \quad (\text{A } 12)$$

Considering Eqs. (3.1,A 6), the solution is

$$\begin{aligned} \omega B_{1Y} &= -k E_{1z} \quad \text{and} \quad \phi_{B_{1Y}} = \phi_{E_{1z}} \quad \text{and} \quad \omega B_{1Z} = +k E_{1y} \quad \text{and} \quad \phi_{B_{1Z}} = \phi_{E_{1y}}, \\ \omega B_{2Y} &= -k E_{2z} \quad \text{and} \quad \phi_{B_{2Y}} = \phi_{E_{2z}} \quad \text{and} \quad \omega B_{2Z} = +k E_{2y} \quad \text{and} \quad \phi_{B_{2Z}} = \phi_{E_{2y}}, \end{aligned} \quad (\text{A } 13)$$

and this is equivalent to

$$\begin{aligned} E_{1y} &= +\frac{\omega B_{1Z}}{k} \quad \text{and} \quad \phi_{E_{1y}} = \phi_{B_{1Z}} \quad \text{and} \quad E_{1z} = -\frac{\omega B_{1Y}}{k} \quad \text{and} \quad \phi_{E_{1z}} = \phi_{B_{1Y}}, \\ E_{2y} &= -\frac{\omega B_{2Z}}{k} \quad \text{and} \quad \phi_{E_{2y}} = \phi_{B_{2Z}} \quad \text{and} \quad E_{2z} = +\frac{\omega B_{2Y}}{k} \quad \text{and} \quad \phi_{E_{2z}} = \phi_{B_{2Y}}. \end{aligned}$$

Then,

$$E_y = +\frac{\omega B_{1Z}}{k} \cos(\omega t - kX + \phi_{B_{1Z}}) - \frac{\omega B_{2Z}}{k} \cos(\omega t + kX + \phi_{B_{2Z}}),$$

$$E_z = -\frac{\omega B_{1Y}}{k} \cos(\omega t - kX + \phi_{B_{1Y}}) + \frac{\omega B_{2Y}}{k} \cos(\omega t + kX + \phi_{B_{2Y}}). \quad (\text{A } 14)$$

With Eqs. (3.1,A 6,A 14), the projection in Eq. (A 5) provides Eqs. (3.6).

The numerical simulations were performed at the computing center (DIO) of the Paris-Meudon observatory. Financial help was supplied for this project by CNRS/INSU/PNST (Programme National Soleil Terre).

REFERENCES

- ARANEDA, J. A., MARSCH, E. & F.-VIÑAS, A. 2008 Proton Core Heating and Beam Formation via Parametrically Unstable Alfvén-Cyclotron Waves. *Physical Review Letters* **100** (12), 125003.
- BUTI, B., VELLI, M., LIEWER, P. C., GOLDSTEIN, B. E. & HADA, T. 2000 Hybrid simulations of collapse of Alfvénic wave packets. *Physics of Plasmas* **7**, 3998–4003.
- CHASTON, C. C., BONNELL, J. W., CARLSON, C. W., BERTHOMIER, M., PETICOLAS, L. M., ROTH, I., MCFADDEN, J. P., ERGUN, R. E. & STRANGEWAY, R. J. 2002 Electron acceleration in the ionospheric Alfvén resonator. *Journal of Geophysical Research (Space Physics)* **107** (11), 41–1.
- GÉNOT, V., LOUARN, P. & LE QUÉAU, D. 1999 A study of the propagation of Alfvén waves in the auroral density cavities. *Journal of Geophysical Research (Space Physics)* **104** (13), 22649–22656.
- GÉNOT, V., MOTTEZ, F. & LOUARN, P. 2001 Particle Acceleration Linked to Alfvén Wave Propagation on Small Scale Density Gradients. *Physics and Chemistry of the Earth C* **26**, 219–222.
- GOERTZ, C. K. 1984 Kinetic Alfvén waves on auroral field lines. *Planetary and Space Science* **32**, 1387–1392.
- HASEGAWA, A. & MIMA, K. 1978 Anomalous transport produced by kinetic Alfvén wave turbulence. *Journal of Geophysical Research (Space Physics)* **83** (12), 1117–1123.
- HILGERS, A. 1992 The auroral radiating plasma cavities. *Geophysical Research Letters* **19**, 237–240.
- KNUDSEN, D. J. 2001 Structure, Acceleration, and Energy in Auroral Arcs and the Role of Alfvén Waves. *Space Science Review* **95**, 501–511.
- LOUARN, P., WAHLUND, J. E., CHUST, T., DE FERAUDY, H., ROUX, A., HOLBACK, B., DOVNER, P. O., ERIKSSON, A. I. & HOLMGREN, G. 1994 Observation of kinetic Alfvén waves by the Freja spacecraft. *Geophys. Res. Lett.* **21**, 1847–+.
- LUND, E. J. 2010 On the dissipation scale of broadband ELF waves in the auroral region. *Journal of Geophysical Research (Space Physics)* **115**, 1201.
- LYSAK, R. L. 1991 Feedback instability of the ionospheric resonant cavity. *Journal of Geophysical Research (Space Physics)* **96**, 1553–1568.
- LYSAK, R. L. & SONG, Y. 2003a Kinetic theory of the Alfvén wave acceleration of auroral electrons. *Journal of Geophysical Research (Space Physics)* **108** (4), 6–1.
- LYSAK, R. L. & SONG, Y. 2003b Nonlocal kinetic theory of Alfvén waves on dipolar field lines. *Journal of Geophysical Research (Space Physics)* **108**, 1327–+.
- MÄKELÄ, J. S., MÄLKKI, A., KOSKINEN, H., BOEHM, M., HOLBACK, B. & ELIASSON, L. 1998 Observations of mesoscale auroral plasma cavity crossings with the Freja satellite. *Journal of Geophysical Research (Space Physics)* **103**, 9391–9404.
- MATTEINI, L., LANDI, S., VELLI, M. & HELLINGER, P. 2010 Kinetics of parametric instabilities of Alfvén waves: Evolution of ion distribution functions. *Journal of Geophysical Research (Space Physics)* **115**, 9106.
- MELROSE, D. B. & WHEATLAND, M. S. 2013 Transfer of Energy, Potential, and Current by Alfvén Waves in Solar Flares. *Solar Physics* **288**, 223–240.
- MOTTEZ, F. 2008 A guiding centre direct implicit scheme for magnetized plasma simulations. *Journal of Computational Physics* **227**, 3260–3281.
- MOTTEZ, F. 2012a Non-propagating electric and density structures formed through non-linear interaction of Alfvén waves. *Annales Geophysicae* **30**, 81–95.

- MOTTEZ, F. 2012*b* The role Alfvén waves in the generation of Earth polar auroras. *Proceedings of "Waves and Instabilities in Space and Astrophysical Plasmas" (WISAP) Eilat, Israel, June 19th - June 24th, 2011* .
- MOTTEZ, F., ADAM, J. C. & HERON, A. 1998 A new guiding centre PIC scheme for electromagnetic highly magnetized plasma simulation. *Computer Physics Communications* **113**, 109–130.
- MOTTEZ, F. & GÉNOT, V. 2011 Electron acceleration by an Alfvénic pulse propagating in an auroral plasma cavity. *Journal of Geophysical Research* **116**, A00K15.
- PERSOON, A. M., GURNETT, D. A., PETERSON, W. K., WAITE, JR., J. H., BURCH, J. L. & GREEN, J. L. 1988 Electron density depletions in the nightside auroral zone. *Journal of Geophysical Research (Space Physics)* **93**, 1871–1895.
- SHARMA, R. P. & SINGH, H. D. 2009 Density cavities associated with inertial Alfvén waves in the auroral plasma. *Journal of Geophysical Research (Space Physics)* **114**, 3109.
- SHUKLA, P. K. & STENFLO, L. 1999 Plasma density cavitation due to inertial Alfvén wave heating. *Physics of Plasmas* **6**, 4120–4122.
- SINGH, N. 1992 Plasma perturbations created by transverse ion heating events in the magnetosphere. *Journal of Geophysical Research (Space Physics)* **97**, 4235–4249.
- SINGH, N. 1994 Pondermotive versus mirror force in creation of the filamentary cavities in auroral plasma. *Geophys. Res. Lett.* **21**, 257–260.
- STASIEWICZ, K., BELLAN, P., CHASTON, C., KLETZING, C., LYSAK, R., MAGGS, J., POKHOTILOV, O., SEYLER, C., SHUKLA, P., STENFLO, L., STRELTSOV, A. & WAHLUND, J.-E. 2000 Small Scale Alfvénic Structure in the Aurora. *Space Science Review* **92**, 423–533.
- THOMPSON, B. J. & LYSAK, R. L. 1996 Electron acceleration by inertial Alfvén waves. *Journal of Geophysical Research (Space Physics)* **101**, 5359–5370.
- VOLWERK, M., LOUARN, P., CHUST, T., ROUX, A., DE FERAUDY, H. & HOLBACK, B. 1996 Solitary kinetic Alfvén waves: A study of the Poynting flux. *Journal of Geophysical Research (Space Physics)* **101** (10), 13335–13344.
- WATT, C. E. J. & RANKIN, R. 2008 Electron acceleration and parallel electric fields due to kinetic Alfvén waves in plasma with similar thermal and Alfvén speeds. *Advances in Space Research* **42**, 964–969.
- WATT, C. E. J. & RANKIN, R. 2010 Do magnetospheric shear Alfvén waves generate sufficient electron energy flux to power the aurora? *Journal of Geophysical Research (Space Physics)* **115** (14), 7224–+.
- YUAN, C. & ZONG, Q. 2013 The double-belt outer radiation belt during CME- and CIR-driven geomagnetic storms. *Journal of Geophysical Research (Space Physics)* **118**, 6291–6301.